Enhanced solar evaporation using a photo-thermal umbrella for wastewater management

Akanksha K. Menon[1$], Iwan Haechler[1$], Sumanjeet Kaur[1], Sean Lubner[1] and Ravi S. Prasher[1,2*]

[1] Energy Storage & Distributed Resources Division, Lawrence Berkeley National Laboratory, Berkeley, CA 94720, USA
[2] Department of Mechanical Engineering, University of California, Berkeley, CA 94720, USA

[*] Correspondence to rsprasher@lbl.gov

[$] Denotes equal contributions

Abstract

Zero-Liquid Discharge (ZLD) is an emerging wastewater management strategy that maximizes water recovery for reuse and produces a solid waste, thereby lowering the environmental impact of wastewater disposal. Evaporation ponds harvest solar energy as heat for ZLD, but require large land areas due to low evaporation rates. Here, we demonstrate a passive and non-contact approach to enhance evaporation by more than 100% using a photo-thermal device that converts sunlight into mid-infrared radiation where water is strongly absorbing. As a result, heat is localized at the water's surface through radiative coupling, resulting in a better utilization of solar energy with a conversion efficiency of 43%. The non-contact nature of the device makes it uniquely suited to treat a wide range of wastewater without contamination, and the use of commercial materials enables a potentially low cost and highly scalable technology for sustainable wastewater management, with the added benefit of salt recovery.

The World Economic Forum recognizes water crises as a major global risk that has arisen from the depletion of natural freshwater resources due to agricultural, industrial and municipal use, while generating vast amounts of wastewater.[1] This poses a sustainability challenge that currently threatens four billion people worldwide and is expected to become more severe with population growth and economic development.[2,3] Desalination of seawater and inland brackish water has emerged as a solution to meet this increasing water demand. However, desalination plants produce concentrated brine as a byproduct, disposal of which is detrimental to land vegetation and the aquatic ecosystem, thereby having a significant environmental impact.[4,5] Thus, there has been a push towards maximizing water recovery for reuse from industrial wastewater and desalination brine to achieve Zero Liquid Discharge (ZLD) such that the final waste is a solid. At present, ZLD involves a series of treatment processes that *(i)* reduce the volume of wastewater using membrane-based systems or thermal brine concentrators, and *(ii)* reduce concentrated brine to a solid waste using a crystallizer or an evaporation pond[6] (Supplementary Fig. 1).

The choice for this final step of ZLD depends upon various factors including concentrated brine volume and composition, energy requirement, local climate and land costs.[7,8] A crystallizer is a complex mechanical system that requires high-grade heat and electricity resulting in a large energy consumption and capital cost. Although crystallizers have a small site footprint, their operating costs depend heavily on the composition of wastewater, which can be exorbitant for highly scaling water (*e.g.* wastewater containing large amounts of silica).[9] In contrast, evaporation ponds are artificial brine disposal ponds with very large surface area (>1000 m^2) that harness solar energy to passively evaporate water from any waste stream, resulting in low energy and operating costs. Currently, evaporation ponds are implemented in China, Australia, Europe (Mediterranean), the Middle East and some areas of the U.S. where they are economically viable owing to inexpensive land and a suitable climate (arid or semi-arid, high solar flux).[6,9,10] Although they offer a tremendous advantage of being suitable for different wastewater streams, capital costs are high due to the large land footprint required for natural evaporation. This

footprint is inversely proportional to the evaporation rate, which is inherently low due to the passive nature and inefficient use of solar energy in these ponds. To reduce environmental impact (*i.e.*, smaller areal footprint) and capital costs, evaporation enhancement in brine disposal ponds is essential, and different approaches have been implemented in this regard.[11,12]

Active methods of enhancement include Wind-Aided Intensified Evaporation (WAIV) and droplet spraying, while passive techniques include the use of solar radiation absorbing organic dyes, wetted floating fins and salt tolerant plants.[7,8,12] These methods have been shown to enhance evaporation rates by up to 35%, while WAIV has shown a 50% enhancement at high salinities but requires continuous electric pumping making it an active system. Recently, a new passive approach for solar evaporation enhancement has emerged where the emphasis is to avoid wastefully heating a large volume of water and instead perform surface heating by localizing solar heat at the water–air interface.[13,14] Various prototypes using nanomaterial-based absorbers and bio-inspired structures exploiting surface heating have since been reported, with solar-vapor conversion efficiencies of over 90% for these floating structures.[15-20] While these devices are suitable for solar stills and steam generation applications, their continuous operation in high salinity wastewater (such as evaporation ponds) causes salt precipitation at the surface in contact with water, resulting in deterioration of the optical and wicking properties over time.[16] Thus, there is a need to develop *non-contact* and *passive* technologies for enhanced solar evaporation that can reduce the footprint of evaporation ponds and eliminate contamination from fouling and scaling. Recently, Cooper et al. proposed a non-contact device for solar steam generation,[21] however their design was focused on generating superheated steam, rather than increasing evaporation rates which is critical to achieve a low cost ZLD technology. Furthermore, given the large areas of evaporation ponds, design simplicity and scalability are key considerations.

Here, we demonstrate a novel and scalable surface heating approach that enhances evaporation by over a 100% under one sun (1000 W m^{-2}), with the potential to increase evaporation by 160% compared to traditional evaporation ponds through optimized thermal design. The system relies solely on radiative

coupling using a photo-thermal conversion device that comprises a selective solar absorber and a blackbody emitter. Since this photo-thermal device shields the water in an evaporation pond from direct sunlight, we refer to it as a "solar umbrella." We design a lab-scale prototype to experimentally demonstrate the potential of the solar umbrella to enhance evaporation from concentrated brines. Using thermal models validated by these lab-scale experiments as well as outdoor testing under natural sunlight, we predict the performance of a large-scale evaporation pond for sustainable wastewater disposal. By enhancing the evaporation two-fold,[22] the land required for disposing the same volume of wastewater is halved, which has a significant environmental impact.

Radiative heat localization

Efficient utilization of solar energy for evaporation is limited by the transparency of water at visible and near-IR wavelengths owing to its low absorption coefficient of 0.01 m^{-1} (Supplementary Note 1). In other words, a depth of 100 m is required for complete absorption of solar radiation by water,[23] while traditional evaporation ponds have typical depths ranging from 0.5 – 2 m.[24] In this case, a large fraction (~60%) of incident solar flux is used in the volumetric or sensible heating of bulk water as shown in Figure 1a. Although the temperature of water increases as sunlight is absorbed, that increase is distributed in the whole volume of liquid (large thermal mass) resulting in a lower temperature at the water surface, as compared to the case where all the radiation is absorbed at the surface. As a result, the transient thermal response of traditional evaporation ponds is slow, which when coupled with the diurnal variation of solar radiation, results in low evaporation rates. At mid-IR and larger wavelengths however, the absorption coefficient of water increases by several orders of magnitude to 10^4 m^{-1}, and consequently, radiation is absorbed within a 100 μm layer, *i.e.*, heat is localized at the surface. Given that evaporation is a surface phenomenon, by shifting solar radiation to mid-IR and larger wavelengths, higher surface temperatures can be achieved, which in turn enhances the evaporation rate. This mid-IR radiation can be obtained from a heated blackbody - as an example, a blackbody with a temperature <150 °C emits ~99.9% of radiation at wavelengths above 2 μm that is absorbed in a thin layer of water

~100 μm (Supplementary Fig. 2). We achieve the shifting of solar radiation to mid-IR wavelengths by utilizing a photo-thermal converter comprising a selective solar absorber and a blackbody emitter shown in Figure 1b. When used as a solar umbrella over a water surface such as an evaporation pond, the overall system efficiency (η) is:

$$\eta = \left(\frac{\dot{m}h_{fg}}{q_{solar}}\right) = \eta_1 \times \eta_2 \times \eta_3 = \left(\frac{\alpha_s q_{solar} - \varepsilon_s \sigma T_{abs}^4}{q_{solar}}\right)\left(\frac{F\varepsilon_b \sigma T_{abs}^4}{\alpha_s q_{solar} - \varepsilon_s \sigma T_{abs}^4}\right)\left(\frac{\dot{m}h_{fg}}{F\varepsilon_b \sigma T_{abs}^4}\right) \quad (1)$$

where $\dot{m}$ is the water evaporation rate, h_{fg} is the latent heat of vaporization and q_{solar} is the incident solar flux. There are three parts to this efficiency: η_1 represents the absorber optical efficiency, η_2 incorporates the emitter efficiency as well as the radiative coupling between the solar umbrella and water surface, and η_3 represents the fraction of incident radiation on the water surface that is used in evaporation.

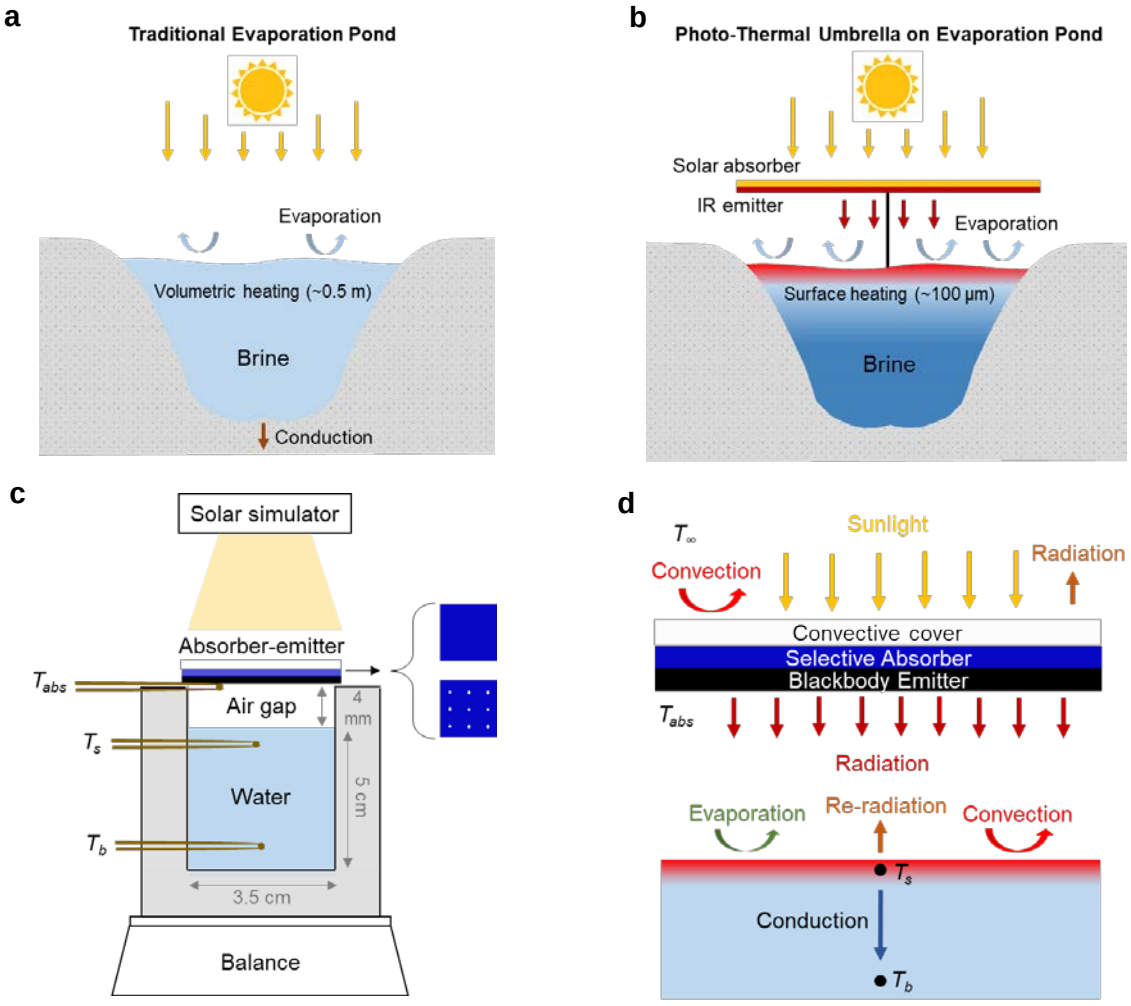

Fig 1: Surface heating using a photo-thermal (solar) umbrella. a Schematic of a conventional evaporation pond where incoming sunlight is volumetrically absorbed, causing a bulk water temperature increase that leads to evaporation. **b** Rendering of the proposed solar umbrella (spectrally selective absorber and blackbody emitter) that converts incoming sunlight into mid-IR radiation where water is strongly absorbing, thereby increasing surface temperature and evaporation rate while the bulk remains at a lower temperature. **c** Schematic of the lab-scale prototype of an evaporation pond comprising water in an acrylic tank separated from the solar umbrella by an air gap and tested under a solar simulator. **d** Energy balance and modes of heat transfer for the umbrella and water, where the red region represents non-contact heat localization at the surface.

Equation (1) can be used to guide the material selection and design of the solar umbrella. To obtain a high η_1 (*i.e.*, to minimize optical losses), the top surface of the umbrella is coated with a spectrally selective solar absorber characterized by a high solar absorbtance, α_s, from 0.2 – 2.5 μm and a near-zero thermal emittance, ε_s, at wavelengths larger than 2.5 μm[25] (Supplementary Note 2 and Supplementary Fig. 3). This reduces radiation losses to the ambient and achieves efficient conversion of sunlight into heat at an equilibrium temperature of T_{abs}. To obtain a high η_2 (*i.e.*, low thermal losses from the photo-thermal converter), the bottom surface of the umbrella is coated with a black emitter characterized by a high IR emittance, ε_b, which is placed above the water surface with a large radiation view factor, F; σ is the Stefan-Boltzmann constant. Furthermore, a convective cover can be used to reduce losses from the surface of the umbrella as it heats up. Finally, to obtain a high η_3, thermal losses from water via conduction, convection and radiation must be minimized such that a majority of the energy is used for evaporation. To test the effectiveness of the non-contact surface heating approach, we designed a lab-scale prototype shown in Figure 1c that consists of two sub-systems, namely the solar umbrella and a water tank that represents an evaporation pond. Figure 1d shows the energy balance for the overall system in a real application.

Lab-scale demonstration

In the lab-scale prototype shown in Figure 1c, the solar umbrella is positioned above the water surface to obtain a view factor larger than 0.8 (Supplementary Note 3 and Supplementary Fig. 4). Under one-sun illumination from a solar simulator (1000 W m^{-2}), the temperature of the solar umbrella increases rapidly and reaches a steady-state value of T_{abs} = 70 °C in less three minutes (Supplementary Fig. 5). The

corresponding increase in the temperature of pure water due to radiative heating from the hot emitter is shown in Figure 2a. The water surface temperature rises steadily from 22.5 °C to 40 °C in one hour, while the bulk water temperature increases only by 2.5 °C in that period. To mimic concentrated wastewater in evaporation ponds, the experiment was repeated with a saturated salt solution (25 wt. % NaCl), which has over 7x the concentration of seawater. Similar trends were observed for the brine, with a 20 °C temperature rise at its surface in one hour, thereby demonstrating radiative heat localization using the solar umbrella. The presence of salts such as NaCl that absorb near-IR radiation increases the brine temperature ~2 °C higher than pure water. To facilitate a comparison with traditional evaporation ponds where water is illuminated directly by sunlight, the same setup was used without the solar umbrella, and corresponding temperatures are shown in Figure 2b. In this case, due to the small absorption coefficient of water at solar wavelengths, the solar flux is volumetrically absorbed resulting in only a 5 °C temperature rise throughout the water in one hour.

Given that evaporation varies with surface temperature, the mass change due to evaporation was measured for each case at an ambient temperature, T_∞ = 25 °C and a relative humidity of 50%. Figure 2c shows the evaporation rates under one sun after subtracting the evaporation in an otherwise identical but dark environment (0.07 kg m^{-2} h^{-1}). Without the solar umbrella, pure water absorbs sunlight volumetrically that increases evaporation to 0.3 kg m^{-2} h^{-1} compared to the dark case (Supplementary Fig. 5). With the solar umbrella however, the evaporation increases to 0.62 kg m^{-2} h^{-1} as a higher surface temperature is achieved; this represents over a two-fold enhancement under the same input solar flux in this passive system. The evaporation rate and surface temperature achieved here are comparable to other surface heating approaches in literature that use self-supporting floating structures (single layer absorbing devices without an insulating foam).[26-28] The saturated NaCl brine showed an evaporation rate of 0.49 kg m^{-2} h^{-1} with surface heating compared to 0.22 kg m^{-2} h^{-1} with bulk heating, both of which represent a ~21% reduction compared to pure water. This is expected as vapor pressure decreases with salinity but is partially compensated by the higher temperature of brine compared to pure water; we note

that this reduction is for an extreme case as the salt concentration is at its saturation limit. To demonstrate continuous operation, brine evaporation experiments were performed for a 3-hour period under a constant solar flux of 1000 W m^{-2} resulting in precipitation and recovery of salts, as shown in Figure 2d. The effect of the photo-thermal umbrella on water evaporation was also investigated under low optical concentrations of 2, 3 and 5 suns. As expected, higher evaporation rates up to 1.6 kg m^{-2} h^{-1} were measured at higher input fluxes (Supplementary Fig. 6). These low optical concentrations can be achieved with passive non-tracking concentrators.[29]

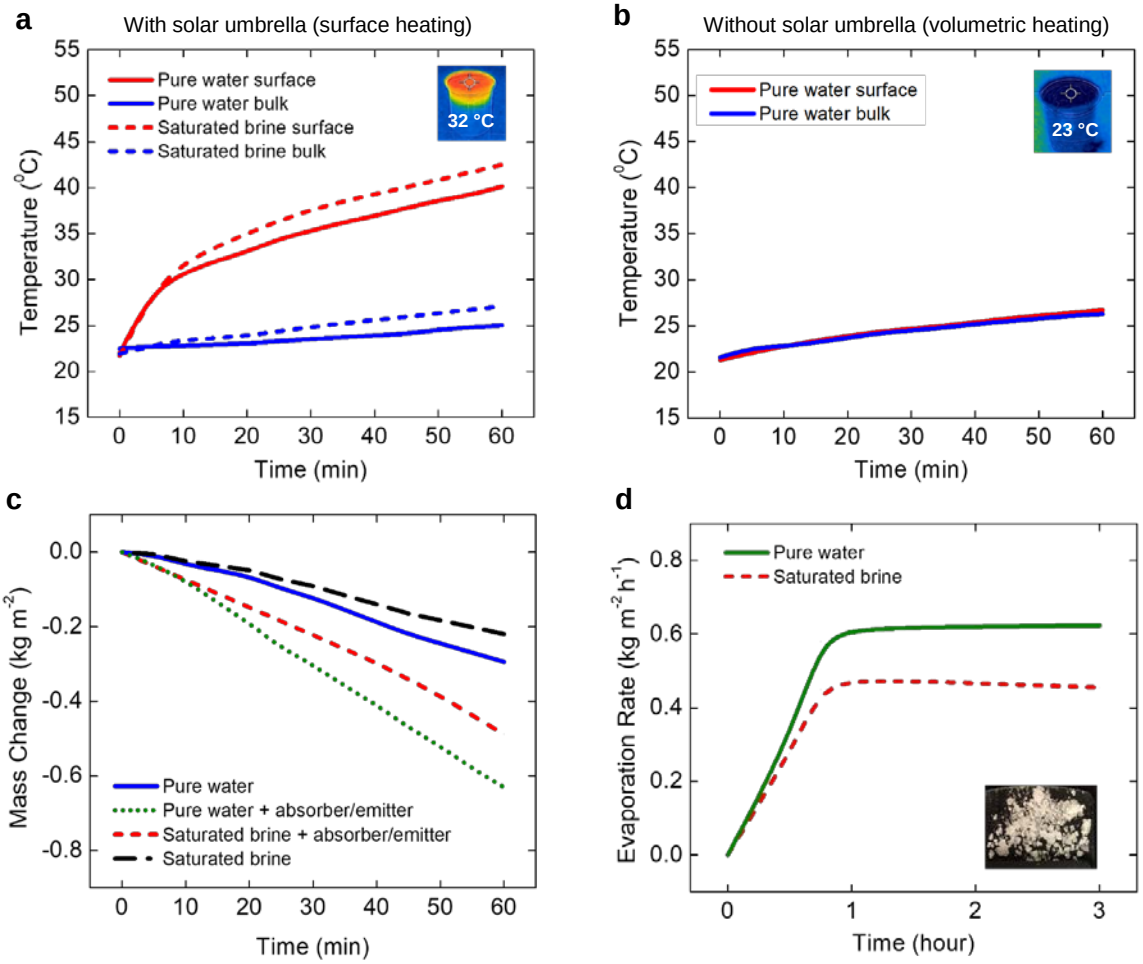

Fig. 2: Lab-scale experimental results. a Surface and bulk temperature of pure water (solid line) and 25 wt. % NaCl brine (dashed line) over one hour with the solar umbrella showing localized heating at the surface. **b** Surface and bulk temperatures of pure water without the solar umbrella showing volumetric heating. Inset images are captured using an IR camera after 10 minutes of illumination for visualization of surface vs. volumetric heating with and without the solar umbrella, respectively (IR images are for qualitative observation only; temperature measurements were made with thermocouples as shown in Fig. 1c). **c** Mass change due to evaporation for pure water under direct illumination (volumetric heating)

compared to evaporation of pure water and NaCl brine with the solar umbrella (surface heating). **d** Evaporation rate over a three-hour period with the solar umbrella for pure water (solid line) and 25 wt. % brine (dashed line) showing a 21% reduction due to salinity. The inset shows precipitated salt crystals from the walls of the water tank owing to evaporation of water from brine to achieve ZLD. All experiments are conducted under one sun (1000 W m^{-2}) at an ambient temperature of 25 °C and relative humidity of 50%.

For the case of pure water, the experimentally measured values are used to calculate sub-system efficiencies from Equation (1): η_1 = 91% η_2 = 74% and η_3 = 63%, resulting in an overall solar-thermal evaporation efficiency of 43% under one sun. This compares favorably with single-layer floating evaporation structures[20,30] and has the added benefit of being non-contact thus eliminating contamination from the wastewater. The absorber efficiency of 91% can be explained by accounting for optical losses due to reflection (5%) and thermal radiation (4%) from the selective absorber surface. The emitter efficiency of 74% is due to an emittance view factor less than unity (ε_b = 0.94 and F ~0.85) in the lab-scale prototype, as well as convection losses from the umbrella. The latter can be minimized with a sophisticated convective cover design or with an evacuated absorber that is commonly used in domestic solar hot water heaters. Finally, an evaporation efficiency of 63% indicates that thermal losses via conduction, convection and radiation from the water compete with and reduce the energy available for evaporation (Supplementary Fig. 8). Furthermore, mass transport is hindered by the closeness of the umbrella to the water surface resulting in a diffusion-limited prototype, as discussed in the modeling section (Supplementary Note 4). This yields an overall solar-thermal evaporation efficiency of 43% which is higher than the 24.6% efficiency of the contactless solar evaporation structure,[21] owing to higher evaporation rates achieved with the solar umbrella (Supplementary Note 7 and Supplementary Table 1). Furthermore, the solar-thermal efficiency of volumetrically heated water, *i.e.,* without the umbrella, under the same solar flux is ~20% based on the experimentally measured evaporation rate (Figure 2c), which is consistent with literature.[18] This confirms the superior performance of surface-based heating for solar evaporation.

Brine evaporation under natural sunlight

To demonstrate continuous or long-term operation with high salinity wastewater (25 wt. % NaCl solution) and to validate the performance of the solar umbrella in real conditions (varying solar flux and wind), brine evaporation experiments were performed for five days under natural sunlight in Berkeley, California as shown in Figure 3a. The solar flux was recorded over an 8-hour period and averaged over all five days as shown in Figure 3b, the corresponding temperature of the umbrella and water surface are displayed in Figure 3c. Under a peak solar flux of 750 W m^{-2}, the solar umbrella temperature rises to 75 °C, which in turn results in a water surface temperature of over 45 °C. Evaporation occurs at the water surface and the generated vapor diffuses into the air gap and through the holes in the umbrella, leaving behind salt deposits along the walls of the acrylic tank. There is no visible contamination or salt deposition on the emitter surface even after several days (Supplementary Fig. 7). This confirms that the solar umbrella can be used as a fouling-resistant device for brine concentration towards zero-liquid discharge.

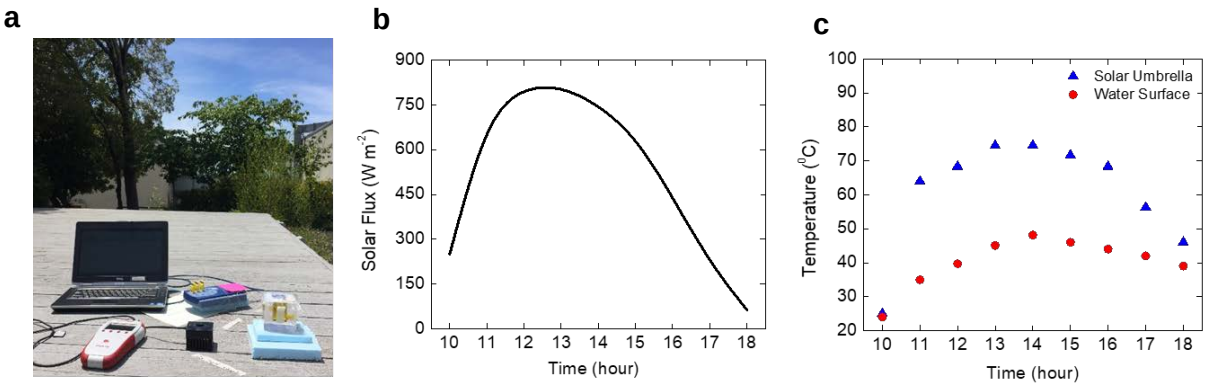

Fig. 3: Outdoor testing of solar umbrella. a Photo of the experimental setup for water evaporation from a saturated salt solution (25 wt% NaCl) over five days. **b** Solar flux measured over an 8-hour window in Berkeley, CA. **c** Temperature of the solar umbrella (emitter) and brine surface corresponding to the solar flux. All experiments are conducted under natural sunlight in Berkeley, CA at an ambient temperature of 20-24 °C and relative humidity of 40-50%.

Thermal model validation

To estimate heat losses in the lab-scale prototype and to make predictions for optimized device design, a thermal model was developed using COMSOL Multiphysics (Supplementary Note 5). The evaporation was modeled as a boundary heat flux:

(2)

$$q_{evap} = h_{evap}(T_s - T_\infty) = \dot{m}h_{fg}$$

where q_{evap} is the heat loss due to evaporation characterized by an effective heat transfer coefficient, h_{evap} (which is a function of temperature). Using the experimentally measured $\dot{m}$ and T_s values obtained at different optical concentrations (Supplementary Fig. 6), an average value of h_{evap} = 28 W m^{-2} K^{-1} is extracted, which is within the range of reported values for floating structure prototypes.[13] The low value corresponds to a diffusion-limited evaporation process,[19,31] which is attributed to the large mass transport resistance owing to the geometry of the lab-scale prototype (Supplementary Fig. 9 and 10).

The simulated cross-sectional temperature profile of water in the acrylic tank receiving infrared radiation from the hot emitter at steady-state is shown in Figure 4a. Heat localization results in a higher temperature of 42 °C at the surface, while the bulk temperature remains close to ambient at 25 °C. Figure 4b shows the transient temperature over an hour, which matches the experimentally measured values, thereby confirming the validity of the thermal model. From this analysis, conduction from the water surface into underlying bulk water was calculated to be 21%, convection from the walls of the acrylic tank was 6%, and radiation from the walls was 11%. This leaves 62% of the energy incident on the water surface for evaporation, which is in good agreement with η_3 obtained from the experimentally measured evaporation rate. We note here that due to the small size of the lab-scale prototype, side walls of the acrylic tank contribute to a 17% parasitic loss (convection and radiation) implying that higher evaporation efficiencies are achievable in a larger system.

Next, the validated thermal model is used to make performance predictions under different conditions. For instance, on cloudy or winter days, when the solar flux can be as low as 300 W m^{-2}, the umbrella can still reach 45 °C and heats the water surface to enhance evaporation. Furthermore, by eliminating convective losses from the umbrella surfaces (*e.g.* evacuated absorber), the steady-state temperature of the solar umbrella can exceed 100 °C under one sun as shown in Figure 4c. This in turn increases blackbody emission to the water surface, resulting in a temperature rise of over 50 °C at its surface as

shown in Figure 4d. Given that the vapor pressure of water increases by 70% from 40 to 50 °C, higher efficiencies and evaporation rates can be obtained using an evacuated umbrella.

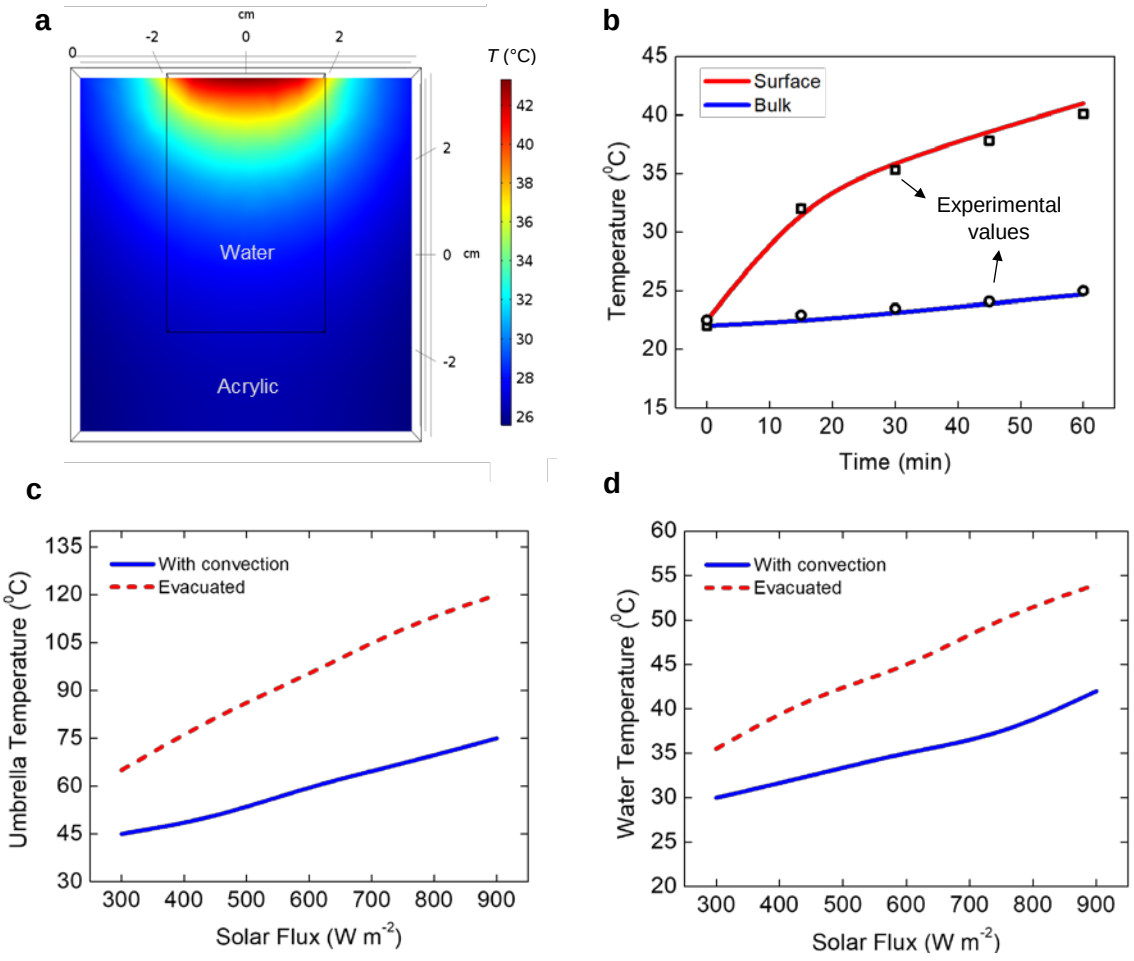

Fig. 4: Thermal model validation and performance prediction for Solar Umbrella. a Cross-sectional temperature profile of water in an acrylic tank with solar umbrella modeled using COMSOL that shows localized heating to a steady state surface temperature of 42 °C due to a large absorption coefficient (10^4 m^{-1}) at mid-IR wavelengths. **b** Water surface and bulk temperatures simulated over one hour (solid lines) and overlaid with experimentally measured temperatures (open symbols) that confirms the validity of the thermal model. **c** Simulated temperature of the solar umbrella at various solar fluxes indicate that convection losses limit the performance, and **d** the corresponding simulated water surface temperature predictions show that even at low solar fluxes, the water surface temperature increases and can reach 55 °C if an evacuated system is used.

Performance prediction for evaporation ponds

The validated thermal model can also be applied to predict the performance of the solar umbrella on large-area evaporation ponds. In existing ponds, the diurnal variation of solar radiation causes a time delay of a few hours between the highest solar intensity and maximum brine temperature as sunlight is

volumetrically absorbed and used for the sensible heating of water. As a result, the transient response is slow and the evaporation rate is small, thereby requiring large land areas to dispose wastewater. In evaporation ponds having a white salt precipitate layer at the bottom, this is exacerbated due to further losses by reflection and conduction to the ground,[32] resulting in even lower solar-thermal evaporation efficiencies. A common approach to address this is the addition of colored organic dyes (*e.g.,* naphthol green and methylene blue) that increase the solar absorption of water during the day. This method has been shown to create a ~3 °C increase in brine surface temperature which enhances the evaporation by up to 35%, but at night these dyes lead to lower surface temperatures.[32,33] The solar umbrella can serve as an alternative to these colored dyes and minimize the time lag caused by volumetric heating through localizing heat in a small thermal mass at the evaporation surface (Supplementary Fig. 12). In other words, the rapid thermal response of the umbrella under sunlight can increase water surface temperature, thereby increasing evaporation. To investigate the effectiveness of this approach for a real pond, the aforementioned validated COMSOL model was modified to mimic a typical evaporation pond depth of 0.5 m,[7,32] exposed to an ambient of 22 °C and 50% relative humidity. Under one sun, the solar umbrella reaches a steady-state temperature of 70 °C, resulting in a thermal emission of ~750 W m^{-2} to the surface of the pond. The resulting water surface temperature (Supplementary Fig. 11) accounting for losses due to natural convection, evaporation and radiation is shown in Figure 5a. From these temperatures, time dependent evaporation is predicted using:

$$\dot{m} = h_m(\rho_s - \rho_\infty) \quad (3)$$

where h_m is the mass transfer coefficient for evaporation, ρ_s is the combined vapor-air density at the water surface and $\rho_\infty$is the corresponding ambient density. For fixed ambient conditions), ρ_∞ is known, h_m is extracted from lab-scale experiments as an average value of 0.0042 m s^{-1} (comparable with data on evaporation from a stagnant water surface[34]), and an increase in the surface temperature from 20 to 40 °C results in a three-fold increase in ρ_s. This in turn results in a higher evaporation rate as shown in Figure 5a for pure water, where the daily evaporation rate is obtained by integrating the time and temperature-

dependent mass flux yielding ~9.8 kg m^{-2} day^{-1}. To account for the salinity of brines, the evaporation is reduced by 21% to 7.8 kg m^{-2} day^{-1} based on experimentally observed evaporation rates for pure water and saturated NaCl in the lab-scale prototype. However, it has been reported that for a salinity of 25 wt. % and at similar ambient conditions to the one modeled here, evaporation is reduced between 18 – 22%;[35] thus a fixed reduction of 21% is valid for this analysis. We also note that in real ponds h_m can be higher as limitations of the lab-scale prototype are surpassed due to advective mass transport (Supplementary Fig. 10) and due to the presence of wind, as well as other factors such as low humidity in arid regions that increase evaporation. The main advantage of the solar umbrella is its fast response that allows for efficient evaporation during the 8-hour illumination window, with over a 100% enhancement compared to volumetrically heated brines under similar ambient conditions over a diurnal cycle.[35-38] An evacuated umbrella may be used for further performance enhancement as discussed in Figure 4c and 4d, and in this case, a daily evaporation of 14.3 kg m^{-2} day^{-1} can be obtained (or 11.3 kg m^{-2} day^{-1} accounting for brine salinity). This leads to a ~160% enhancement in evaporation compared to traditional ponds, thus surpassing the performance of organic dyes and WAIV, as shown in Figure 5b.

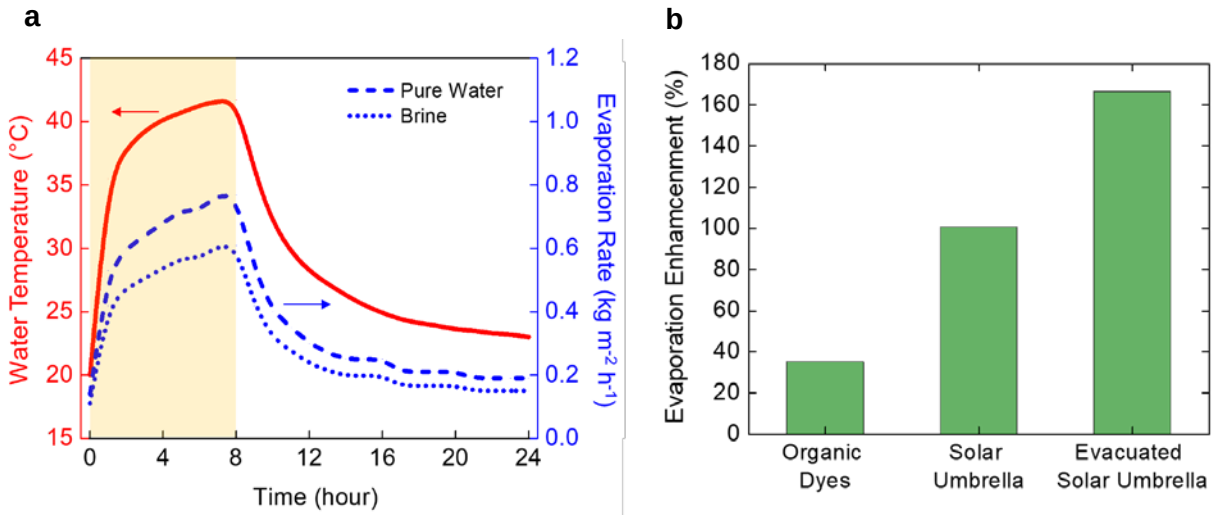

Fig. 5: Simulated performance of evaporation ponds for ZLD. a Simulation of water surface temperature and evaporation rate over a diurnal cycle; the shaded region represents sunlight incident on the solar umbrella, resulting in heat localization at the water surface and a corresponding rise in temperature. The evaporation rate is calculated at each temperature, and the brine evaporation rate under these conditions is obtained as a 21% reduction from pure water evaporation. **b** Daily evaporation enhancement (relative to a traditional volumetrically heated pond under 1 sun) by passive methods

including radiation absorbing dyes, solar umbrella and an evacuated solar umbrella at a relative humidity of 50% and ambient temperature of 20 °C.

Finally, we vary the pond depth to evaluate conditions under which bulk heating can attain temperatures similar to surface heating with the solar umbrella (Supplementary Note 6). The model indicates that a pond depth of ~0.1 cm would be required to compete with surface heating, which is unrealistically small for a ZLD evaporation pond (Supplementary Fig. 12).

In summary, we report a new photo-thermal approach to improve the efficiency of solar evaporation by leveraging the inherently strong infrared absorption of water that causes heat localization in a thin layer (<100 μm) at the surface. The system is passive and non-contact, and comprises a commercially available selective solar absorber and a spray-on black paint emitter. Surface heating results in over a 100% enhancement in evaporation compared to volumetric heating which translates into a lower land requirement, and a 43% solar-thermal efficiency is achieved under one sun. The non-contact radiative coupling eliminates risk of fouling and contamination from wastewater streams, making this system uniquely suited for long-term implementation in brine disposal ponds for achieving zero-liquid discharge, as demonstrated with a saturated salt solution. Furthermore, by reducing thermal losses (primarily convection from the absorber surface), the umbrella temperature can be increased significantly, thereby enabling high temperature vapor or steam generation under one sun. Other potential applications of the photo-thermal umbrella is in solar stills where vapor generated can be condensed to produce drinking water for off-grid communities. The design simplicity lends itself to a scalable solution for the sustainable management and disposal of wastewater.

Methods

Materials and characterization: The selective solar absorber was obtained from Almeco ($TiNOX_{energy}$ on aluminum), which has a solar absorptance of 0.95 and thermal emittance of 0.04 at thermal wavelengths that suppresses radiation losses. The black paint was a high emissivity paint (Zynolyte Hi-Temp Paint, Aervoe) that was sprayed in even three layers on the aluminum substrate and cured at 300 °C in a furnace for two hours to achieve an emittance of 0.94 at infrared wavelengths. The optical properties of the spectrally selective absorber and black paint emitter were measured using an FTIR (Thermo Electron Nicolet 5700), coupled with an integrating sphere accessory (Pike Technologies Mid-IR IntegratIR). As the samples were non-transmitting, the absorptance was calculated as unity minus reflectance.

Experimental setup: For lab-scale prototype testing, a solar simulator (Newport, 94081A) with an optical filter for AM 1.5G spectrum is used as the solar input. A power meter and thermopile detector (Newport, 919P-030-18) were used to measure the incoming solar flux at the same location as the water tank. The tank is made out of acrylic and comprises an inner pocket (square cross-section with a side length of 35 mm and a 50 mm depth) that is coated in a reflective foil and filled with water. The inner pocket is surrounded by a 20 mm thick acrylic wall on all sides that minimizes thermal losses from the sides of the tank. Two K-type thermocouples were placed in the tank: one ~2 mm below the water surface to record the surface temperature, T_s, and one 40 mm below the surface to record the bulk water temperature, T_b. The selective absorber-black emitter was mounted on Teflon spacers and placed ~4 mm above the water surface. Another K-type thermocouple was attached to the surface of the emitter to measure its temperature, T_{abs}, and estimate the blackbody emissive power. Since the substrate is thin ~0.5 mm and metallic, temperatures of the absorber and emitter are equal and remain isothermal over the course of the measurements. A convective shield (bubble wrap) was placed on top of the absorber to reduce convection losses from the hot surface. Holes were drilled in the absorber (covering less than 1% of its area) to allow vapor diffusion into the ambient air. The tank was placed on a balance (A&D, GF-4000) that records the mass loss due to evaporation over time. A hygrometer (Onset, HOBO UX100) was kept

next to the balance to measure ambient conditions (temperature, T_∞ and relative humidity). The K-type thermocouples were connected to a data logger (Pico Technologies, USB TC-08) that records temperature as a function of time. A copper aperture was placed above the absorber to limit extraneous light from the solar simulator during experimental testing. As a first step, evaporation under dark conditions was measured for 30 minutes with the simulator shutter closed. Next, the shutter was opened with the incident flux set to 1000 W m^{-2}, unless specified otherwise. Mass loss and temperature measurements were made for at least two hours, and values reported in the manuscript are averaged over four runs with the dark evaporation subtracted. Laboratory and outdoor experiments were performed at ambient temperatures between 20-24 °C and a relative humidity of 40-50%.

Modeling: A 3D model was developed on COMSOL Multiphysics software to simulate steady-state and transient operating conditions. Both the lab-scale prototype and real evaporation pond simulations were performed using radiation in participating media, and spectral properties of the photo-thermal umbrella were used as inputs along with relevant boundary conditions (Supplementary Note 5).

Data Availability

The data that support the findings of this study are available in the Supplementary Information, and additional data is available from the corresponding author (rsprasher@lbl.gov) upon request.

Acknowledgements

This work was supported by the Laboratory Directed Research and Development Program (LDRD) at Lawrence Berkeley National Laboratory under contract # DE-AC02-05CH11231. The authors thank Dr. Zhi Huang and Sishir Mohammed for assistance with thermal and mass transport modeling, and gratefully acknowledge Almeco for providing selective absorber samples. A.K.M acknowledges funding support from the ITRI-Rosenfeld Fellowship from the Energy Technologies Area at Lawrence Berkeley National Laboratory. I.H. acknowledges funding support from the Zeno Karl Schindler Foundation.

Author Contributions

A.K.M. and I.H. contributed equally to this work. The idea of non-contact radiative heating was conceptualized by R.P. and developed by S.L., S.K. and I.H. A.K.M. and I.H. conducted experiments, developed models and analyzed results. A.K.M., I.H., S.K., and R.P. wrote the paper. R.P supervised the research.

Ethics Declaration

The authors declare no competing interests.

References

1 The Global Risks Report 2018. (World Economic Forum, Geneva, 2018).

2 Grant, S. B. *et al.* Taking the "Waste" Out of "Wastewater" for Human Water Security and Ecosystem Sustainability. *Science* **337**, 681 (2012).

3 Vörösmarty, C. J. *et al.* Global threats to human water security and river biodiversity. *Nature* **467**, 555, doi:10.1038/nature09440

https://www.nature.com/articles/nature09440#supplementary-information (2010).

4 Pinto, F. S. & Marques, R. C. Desalination projects economic feasibility: A standardization of cost determinants. *Renewable and Sustainable Energy Reviews* **78**, 904-915, doi:https://doi.org/10.1016/j.rser.2017.05.024 (2017).

5 Gude, V. G. Desalination and sustainability – An appraisal and current perspective. *Water Research* **89**, 87-106, doi:https://doi.org/10.1016/j.watres.2015.11.012 (2016).

6 Tong, T. & Elimelech, M. The Global Rise of Zero Liquid Discharge for Wastewater Management: Drivers, Technologies, and Future Directions. *Environmental Science & Technology* **50**, 6846-6855, doi:10.1021/acs.est.6b01000 (2016).

7 Morillo, J. *et al.* Comparative study of brine management technologies for desalination plants. *Desalination* **336**, 32-49, doi:https://doi.org/10.1016/j.desal.2013.12.038 (2014).

8 Giwa, A., Dufour, V., Al Marzooqi, F., Al Kaabi, M. & Hasan, S. W. Brine management methods: Recent innovations and current status. *Desalination* **407**, 1-23, doi:https://doi.org/10.1016/j.desal.2016.12.008 (2017).

9 Juby, G. *et al.* Evaluation and Selection of Available Processes for a Zero-Liquid Discharge System. Report No. DWPR No. 149, (U.S. Department of the Interior Bureau of Reclamation, 2008).

10 Mickley, M. Treatment of Concentrate. Report No. DWPR Report No. 155, (U.S. Department of the Interior Bureau of Reclamation, 2008).

11 Ahmed, M., Shayya, W. H., Hoey, D. & Al-Handaly, J. Brine Disposal from Inland Desalination Plants. *Water International* **27**, 194-201, doi:10.1080/02508060208686992 (2002).

12 Hoque, S., Alexander, T. & Gurian, P. L. Innovative Technologies Increase Evaporation Pond Efficiency. *IDA Journal of Desalination and Water Reuse* **2**, 72-78, doi:10.1179/ida.2010.2.1.72 (2010).

13 Ghasemi, H. *et al.* Solar steam generation by heat localization. *Nature Communications* **5**, 4449, doi:10.1038/ncomms5449

https://www.nature.com/articles/ncomms5449#supplementary-information (2014).
14 Tao, P. *et al.* Solar-driven interfacial evaporation. *Nature Energy*, doi:10.1038/s41560-018-0260-7 (2018).
15 Shi, Y. *et al.* Solar Evaporator with Controlled Salt Precipitation for Zero Liquid Discharge Desalination. *Environmental Science & Technology* **52**, 11822-11830, doi:10.1021/acs.est.8b03300 (2018).
16 Ni, G. *et al.* A salt-rejecting floating solar still for low-cost desalination. *Energy & Environmental Science* **11**, 1510-1519, doi:10.1039/C8EE00220G (2018).
17 Xu, N. *et al.* Mushrooms as Efficient Solar Steam-Generation Devices. *Advanced Materials* **29**, 1606762, doi:10.1002/adma.201606762 (2017).
18 Finnerty, C., Zhang, L., Sedlak, D. L., Nelson, K. L. & Mi, B. Synthetic Graphene Oxide Leaf for Solar Desalination with Zero Liquid Discharge. *Environmental Science & Technology* **51**, 11701-11709, doi:10.1021/acs.est.7b03040 (2017).
19 Ni, G. *et al.* Steam generation under one sun enabled by a floating structure with thermal concentration. *Nature Energy* **1**, 16126, doi:10.1038/nenergy.2016.126

https://www.nature.com/articles/nenergy2016126#supplementary-information (2016).
20 Bae, K. *et al.* Flexible thin-film black gold membranes with ultrabroadband plasmonic nanofocusing for efficient solar vapour generation. *Nature Communications* **6**, 10103, doi:10.1038/ncomms10103

https://www.nature.com/articles/ncomms10103#supplementary-information (2015).
21 Cooper, T. A. *et al.* Contactless steam generation and superheating under one sun illumination. *Nature Communications* **9**, 5086, doi:10.1038/s41467-018-07494-2 (2018).
22 Menon, A. K., Haechler, I., Kaur, S., Lubner, S. & Prasher, R. S. Enhanced solar evaporation using a photo-thermal umbrella: towards zero liquid discharge wastewater management. *eprint arXiv:1905.10394*, arXiv:1905.10394 (2019).
23 Segelstein, D. J. *The complex refractive index of water*, University of Missouri-Kansas City, (1981).
24 Principles of Design and Operations of Wastewater Treatment Pond Systems for Plant Operators, Engineers, and Managers. (2011).
25 Cao, F., McEnaney, K., Chen, G. & Ren, Z. A review of cermet-based spectrally selective solar absorbers. *Energy & Environmental Science* **7**, 1615-1627, doi:10.1039/C3EE43825B (2014).
26 Shi, L., Wang, Y., Zhang, L. & Wang, P. Rational design of a bi-layered reduced graphene oxide film on polystyrene foam for solar-driven interfacial water evaporation. *Journal of Materials Chemistry A* **5**, 16212-16219, doi:10.1039/C6TA09810J (2017).
27 Ye, M. *et al.* Synthesis of Black TiOx Nanoparticles by Mg Reduction of TiO2 Nanocrystals and their Application for Solar Water Evaporation. *Advanced Energy Materials* **7**, 1601811, doi:10.1002/aenm.201601811 (2016).
28 Zhang, L., Tang, B., Wu, J., Li, R. & Wang, P. Hydrophobic Light-to-Heat Conversion Membranes with Self-Healing Ability for Interfacial Solar Heating. *Advanced Materials* **27**, 4889-4894, doi:10.1002/adma.201502362 (2015).
29 Winston, R. Principles of solar concentrators of a novel design. *Solar Energy* **16**, 89-95, doi:https://doi.org/10.1016/0038-092X(74)90004-8 (1974).
30 Wang, Z. *et al.* Bio-Inspired Evaporation Through Plasmonic Film of Nanoparticles at the Air–Water Interface. *Small* **10**, 3234-3239, doi:10.1002/smll.201401071 (2014).
31 Hisatake, K., Tanaka, S. & Aizawa, Y. Evaporation rate of water in a vessel. *Journal of Applied Physics* **73**, 7395-7401, doi:10.1063/1.354031 (1993).
32 Bloch, M. R., Farkas, L. & Spiegler, K. S. Solar Evaporation of Salt Brines. *Industrial & Engineering Chemistry* **43**, 1544-1553, doi:10.1021/ie50499a025 (1951).

33 Gunaji, N. N., Keyes, C. G., New Mexico State, U. & United, S. *Disposal of brine by solar evaporation*. (U.S. Dept. of the Interior, Office of Saline Water, 1968).
34 Marek, R. & Straub, J. Analysis of the evaporation coefficient and the condensation coefficient of water. *International Journal of Heat and Mass Transfer* **44**, 39-53, doi:https://doi.org/10.1016/S0017-9310(00)00086-7 (2001).
35 Harbeck Jr, G. E. The effect of salinity on evaporation. Report No. 272A, (1955).
36 Langbein, W. B. & Harbeck, G. E. Studies of Evaporation. *Science* **119**, 328 (1954).
37 Moore, J. & Runkles, J. R. Evaporation from Brine Solutions under Controlled Laboratory Conditions. Report No. 77, (1968).
38 Turk, L. J. Evaporation of Brine: A Field Study on the Bonneville Salt Flats, Utah. *Water Resources Research* **6**, 1209-1215, doi:10.1029/WR006i004p01209 (1970).